International Journal of Thermofluids 1–2 (2020) 100010

Contents lists available at ScienceDirect

International Journal of Thermofluids

journal homepage: www.elsevier.com/locate/ijtf

Heat and mass transfer for a small diameter thermosyphon with low fill ratio

Anthony J. Robinson[a,*], Kate Smith[a], Turlough Hughes[a], Sauro Filippeschi[b]

[a] Department of Mechanical and Manufacturing Engineering, Trinity College Dublin, Dublin D2, Ireland
[b] Department of Energy, Systems, Land and Constructions Engineering, University of Pisa, Pisa, Italy

ARTICLE INFO

Article History:
Received 23 October 2019
Revised 21 December 2019
Accepted 21 December 2019
Available online 26 December 2019

Keywords:
Flow regimes
Flow visualization
Heat transfer
Reflux Thermosyphon

ABSTRACT

Thermosyphons of smaller dimensions are more commonly sought after as electronics cooling devices. The interactions of the tube wall and working fluid become more significant as the dimension of a thermosyphon is reduced, particularly for high surface tension fluids such as water. This paper aims to experimentally investigate a water-charged, small diameter (8 mm) thermosyphon as it operates with a low (25%) filling ratio for a relatively long evaporator length of 200 mm. High speed videography provides in-situ flow pattern visualization at different heat input power. The boiling regimes for each level of heat flux are determined by analyzing the flow patterns from the high-speed video footage. The interdependence of the flow regimes and the heat and mass transfer mechanisms is evaluated using the measured wall temperature variations and derived thermosyphon performance metrics, such as the average heat transfer coefficients and thermal resistances. It was observed that the heat and mass transport was dominated by Geyser-type boiling at lower heat fluxes with associated low heat transfer coefficients in the evaporator and condenser. With increasing thermal power, less liquid was observed to return to the evaporator resulting in more aggressive boiling events which improved the heat transfer coefficients in both the evaporator and condenser. For all power levels tested, the dominant thermal resistance was found to be that associated with the condenser. The ultimate failure of the thermosyphon was a result of liquid hold-up in the condenser section and subsequent falling liquid film and evaporator dryout.

1. Introduction

A thermosyphon is a wickless, gravity-assisted heat pipe filled with working fluid in saturated equilibrium. Thermosyphons are widely used in electronics cooling systems, solar photovoltaic cells, HVAC and energy recovery systems due to their simple structure and capability to remove high heat fluxes with low temperature differentials [1–7].

Reflux thermosyphons are possibly the simplest thermosyphon architecture. Within a sealed container, typically a tube, working fluid under a partial vacuum is evaporated in the region of the evaporator, where heat is applied to the external container wall. The mode of two phase heat transfer in the evaporator depends on many factors, including the working fluid, thermodynamic state, tube size, heat loading, inclination angle and fill ratio. Regardless, the applied heat is converted to latent heat via the phase change process in the evaporator after which the vapor flows to the condenser region, which is the region where heat is extracted from the external container wall. Here the latent heat is released when the vapor condenses. A necessary condition for conventional reflux thermosyphons is that the evaporator zone is below that of the condenser so that the condensate can flow back to the evaporator by gravitational forces, thus creating a gravity-forced internal flow loop.

Over the past century, a significant volume of research has been devoted to predict the heat transfer performances and transport limits of thermosyphons [1]. The empirical correlations developed are predominantly based on measurements obtained from thermosyphons with high filling ratios (circa 100%) and low confinement effects. The influence of confinement in two phase flows has been gaining more attention in recent times as a result of a progressive reduction in size and increased integration of electronic packages which require compact thermal management systems. Traditionally, confinement is quantified by the ratio of the capillary length of the fluid and the channel hydraulic diameter, formally known as the Confinement number, Cornwell and Kew [8,9];

$$Co = \frac{L_c}{D_H} \tag{1}$$

where

$$L_c = \sqrt{\frac{\sigma}{g(\rho_l - \rho_v)}} \tag{2}$$

* Corresponding author.
E-mail address: arobins@tcd.ie (A.J. Robinson).

https://doi.org/10.1016/j.ijft.2019.100010

Nomenclature

A	area [m^2]
Co	confinement number
Bo	bond number
D	diameter [m]
g	acceleration due to gravity [m^2/s]
h	heat transfer coefficient [W/m^2K]
I	current [A]
k	thermal conductivity [W/mK]
L_c	characteristic bubble length [m]
M	molecular Weight [kg/kmol]
P_r	reduced pressure
P_v	vapor pressure [bar]
q	heat flux [W/m^2]
Q	power [W]
R_{TH}	thermal resistance [K/W]
T	temperature [K]
V	voltage [V]
Greek Symbols	
ρ	density [kg/m^3]
σ	surface tension [N/m]
Subscripts	
a	adiabatic
c	condenser
e	evaporator
i	internal
l	liquid
sat	saturation
w	wall

The rule of thumb is that for Co>0.5 confinement effects are important, though confinement influences have been observed as low as Co~0.35 [10]. Recently, Smith et al. [10,11] investigated varying confinement of two phase reflux thermosyphons and showed that for confinement levels of Co=0.34, pulsatile Geyser boiling occurred which caused unsteady performance with associated heat and mass transfer characteristics very different from the conventional pool boiling – falling film condensation models. The observed flow regimes change markedly with Confinement number ($0.12 \leq Co \leq 0.34$) and the rate of vapor production. The heat transfer coefficient in the evaporator is dependent on the associated flow regime and could be better or worse than that of nucleate pool boiling, which is the generally assumed heat transfer mode when modelling thermosyphons [9].

It is well known in the literature that thermosyphon performance is highly affected by the filling ratio (FR), defined as the ratio between the volume of the working fluid and the volume of the evaporator [12,13]. The filling ratio also influences the operational limitations of the thermosyphon, especially the flooding (entrainment) and dry-out limits [1]. Recent numerical models show that the thermal resistance decreases as the fill ratio decreases [14]. The optimum fill ratio provides the lowest thermal resistance along with the shortest thermal response time [15]. Using this model, the optimum filling ratio was found to be low (FR < 35%), for the particular system tested. However, at low fill ratios dryout of the thermosyphon is easily triggered and occurs at lower input heat fluxes. Dynamic partial dryout has been observed along the evaporator surface and can establish a quasi-steady sub-critical heat flux regime. This numerically determined phenomena has been confirmed by experiments [15]. From the experiments it is found that at low filling ratio the heat transfer is limited by the dryout of the falling liquid film in the zone immediately above the liquid pool.

The above discussion highlights that confinement and fill ratio are important factors in determining the thermal resistance and maximum heat transfer capacity of reflux two-phase thermosyphons. The net thermal power dictates the mass flow rate of the working fluid and subsequent flow regimes, which is sensitive to confinement. However, the evaporator heat flux depends on the thermal power loading and the evaporator surface area, with the latter being a function of the tube inner diameter and the evaporator length. For example, Smith et al. [10,11] and Jafari et al. [15] both studied water charged reflux thermosyphons of overall 500 mm length and similar evaporator lengths (100 mm and 75 mm respectively). However, the former utilized an 8 mm inner diameter tube whereas the latter was 35 mm, such that for the same heat loading the heat fluxes differed considerably.

Notably, the recent work of Smith et al. used FR = 100% of water and determined that the prevalent flow regime was Geyser boiling for all of the heat fluxes tested. The evaporator heat transfer coefficient was measured to be generally poorer than that predicted by the Imura correlation [16] for nucleate boiling in thermosyphons, indicating that this is not an ideal mode of operation. The Jafari et al. [15] tests also observed Geyser boiling for moderate to high fill ratios, though generally only at low applied power loadings. They also observed poorer heat transfer coefficients in the evaporator for this flow regime as compared with the Imura correlation. For low fill ratios Geysering was not observed and the measured heat transfer coefficients were higher.

Evidently, there are many parameters which act together to define the thermal performance of closed two-phase reflux thermosyphons. Of key relevance are the filling ratio, confinement and evaporator length. For confined thermosyphons, such as those studied by Smith et al. [10,11], it is possible that low fill ratios may mitigate Geyser boiling and possibly improve the evaporator heat transfer coefficient by promoting thin film evaporation, as was shown to be the case by Jafari et al. [15].

To this end, this study experimentally investigates a small diameter thermosyphon filled close to the predicted optimal level (FR = 25%) using the same apparatus as Smith et al. [10,11]. Here, a relatively long evaporator length of 200 mm was utilized in order to provide suitable length for possible falling film evaporation to occur whilst at the same time reducing the local heat fluxes for given power loadings. The transparent test section and high-speed imaging allows for the capture and analysis of the flow regimes as the input heat loading is increased to thermosyphon failure. In this way, the heat transfer and failure mode can be directly linked to the boiling dynamics and flow regimes.

2. Experimental apparatus

2.1. Test facility

A primary aim of the current experiments was to fully visualize the two-phase flow patterns in the evaporator section of the thermosyphon. This was achieved by designing and fabricating a completely transparent thermosyphon and test apparatus which provided a transparent heated section without any internal flow restrictions.

The experimental set-up for the tests carried out in this investigation is shown in Fig. 1. The main body of the thermosyphon consists of a length of sapphire tube, 500 mm in length, with 8 mm inner diameter and 1 mm wall thickness. Sapphire was used for the test section because it has a thermal conductivity comparable to that of metals ($k \approx 25-40$ W/mK) and is transparent to light in the visible spectrum (~ 80%). The high thermal conductivity of sapphire is desirable compared to other transparent low conductivity materials, such as glass, because it (i) mitigates large temperature differences across the tube wall, (ii) responds quickly to dynamic changes within the thermosyphon and (iii) offers a low enough thermal resistivity that heat can be extracted from a water-cooled condenser of practical length. The evaporator section length tested here was 200 mm as

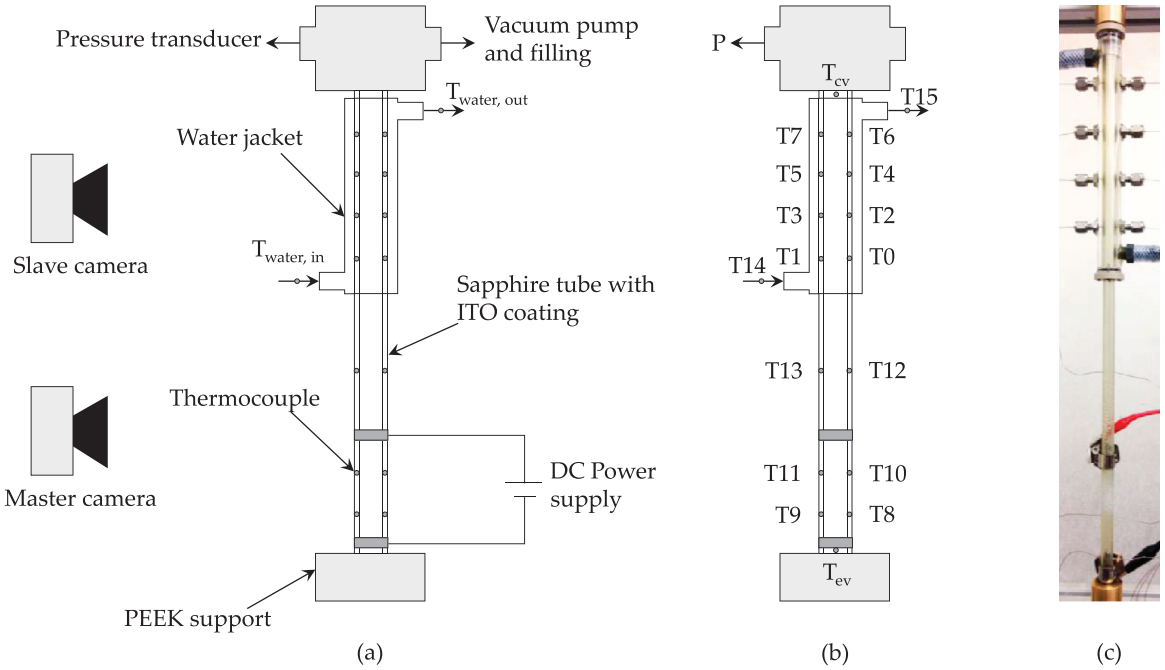

Fig. 1. (a) Schematic of apparatus; (b) Instrumentation of test section; (c) Photographic image of thermosyphon.

was the condenser section length. These sections were separated by an adiabatic section of 100 mm length.

The outer surface of the sapphire tube was coated with a 600 nm of electrically conductive and visually transparent Indium Tin Oxide (ITO).

The evaporator section was ohmically heated by an Elektro-Automatik (8360–10T) DC power supply which imposed a voltage differential across, and subsequent current flow through, the ITO coating. The electrical connection to the tube surface was applied through metal leads, tightly fixed to the surface of the sapphire tube at the desired spacing. The thickness and electrical resistivity of the coating was such that an adequate level of uniform heating could be achieved in the evaporator section, while still allowing full internal visualization of the thermosyphon test section.

The condenser section consisted of a 200 mm long annular and transparent polycarbonate water jacket. The condenser water jacket was connected to a Julabo A40 chiller unit through which the condenser water temperature could be accurately controlled at a desired set point. A sufficiently high cooling water flow rate ensured a low coolant-side thermal resistance so that the condenser wall temperature was maintained close to that of the cooling water, which was nominally 20 °C for all tests. Thermocouples were positioned in the inlet and outlet of the condenser jacket to verify small temperature drops across the condenser section.

2.2. Data reduction and uncertainty

The rate of evaporation is defined by the total thermal power as there is no forced convection of the fluid through the thermosyphon. In order to evaluate the thermal power supplied to the thermosyphon, the input heat applied to the heated evaporator section, Q_{in}, was calculated using the recorded voltage, V, and current, I,

$$Q_{in} = V \cdot I \tag{3}$$

To allow full visual access to the total length of the thermosyphon, no insulation was used on the test section. Due to natural convection and some radiation heat transfer to the surroundings, inevitable heat losses were encountered. These losses were measured to account for the magnitude of heat lost to the surroundings. Measurement of the heat losses consisted of applying a known heat flux to the evaporator section, while the interior was evacuated. Any heat transfer would thus be due to natural convection and radiation to the ambient and a simple correlation was developed. Subsequently, the total heat transferred to the evaporator could be estimated using the following;

$$Q_{tot} = Q_{in} - Q_{loss} \tag{4}$$

Typically, heat losses were less than 15%.

With an accurate estimation of the total thermal power entering the thermosyphon, the interior surface heat flux could then be calculated as,

$$q_n = \frac{Q_{tot}}{A_{i,n}} \tag{5}$$

where the heat flux to the working fluid in the evaporator ($n = e$) can be different from that of the working fluid in the condenser ($n = c$) if the respective surface areas differ, which is not the case here.

The heat transfer coefficient in the evaporator section, h_e, is calculated using q_e and the time averaged internal saturation temperature measured in the fluid of the evaporator and time and spatial averaged evaporator wall section temperatures ($\Delta T = T_{ew} - T_{sat}$);

$$h_e = \frac{q_e}{(T_{ew} - T_{sat})} \tag{6}$$

The heat transfer coefficient of the condenser section, h_c, is estimated based on q_c and the temperature difference between the fluid saturation temperature and the time and spatial condenser wall temperature, ($\Delta T = T_{sat} - T_{cw}$), where the condenser wall temperature was held constant at T_{cw}=21 °C for each test;

$$h_c = \frac{q_e}{(T_{sat} - T_{cw})} \tag{7}$$

It should be noted that the internal working fluid temperature, here represented as T_{sat}, was measured by the thermocouple immersed the evaporator fluid and requires some comment. Although a thermocouple was also inserted in the condenser, this reading is not always reliable due to subcooled condensate interacting with the probe, which is particularly problematic when liquid hold-up occurs in the condenser i.e. when a volume of liquid is trapped in the top region of the condenser. However, the use of T_{sat}, as characterized by the evaporator thermodynamic state, is justified here due to two reasons.

As will be discussed, the low to medium heat flux cases studied here showed flow regimes whereby liquid from the evaporator is in fact propelled into the condenser (Geyser, Partial Geyser and Breach flow regimes). Furthermore, calculating the vapor core thermal resistance using the conventional method [17] whereby the hydraulic pressure drop between the evaporator and condenser is calculated resulting in a drop in the saturation temperature, the effective vapor core thermal resistance is circa two orders of magnitude lower than those associated with the evaporator and condenser thermal resistances for all tests. It is also worth noting that, as stated, the fixed parameter between tests was the condenser wall temperature, and as such the thermodynamic state of the fluid varied with an increase in saturation temperature and pressure occurring with increasing applied power. For the range of power tested here the saturation temperature ranged between 30 °C and 44 °C.

Since radial and axial thermal resistances associated with the sapphire are negligibly small, the effective thermal resistances of the evaporator and condenser are;

$$R_{TH,e} = \frac{1}{h_e A_{i,e}} \tag{8}$$

and,

$$R_{TH,c} = \frac{1}{h_c A_{i,c}} \tag{9}$$

such that the overall thermal resistance of the thermosyphon is the addition of the two,

$$R_{TH,tot} = R_{TH,e} + R_{TH,c} \tag{10}$$

The experimental uncertainty of each measured quantity is listed in Table 1. The propagation of these uncertainties to the calculated quantities was determined according the method outlined by Kline and McClintock [18]. Using the associated measurement errors in Table 1, the uncertainty in the calculation of the heat transfer coefficient and thermal resistances was estimated not to exceed ± 10%.

3. Results and discussion

3.1. Flow patterns

The primary aim of this investigation is to gain insight into the heat transfer mechanisms of two phase closed thermosyphons by focusing on flow regimes and flow patterns. This is not the conventional approach as it does not oversimplify the averaged flow mechanics and subsequent heat transfer mechanisms into pool boiling and/or thin film evaporation in the evaporator, combined with falling film condensation in the condenser. Although these mechanisms may be relevant for large diameter thermosyphons, they may not be inappropriate for small diameter systems where confinement effects are important [10,11]. For the thermosyphon considered here, the Confinement Number is Co ~ 0.34 which is large enough to be considered a confined two-phase system [10].

Fig. 2 shows the influence of the applied thermal power on the wall temperature of the evaporator. Here the temperature at the lowest measurement point has been plotted (T_{e1}) and is illustrative of the other evaporator measurement points. The dynamics of the evaporator are very sensitive to applied thermal power. For the lowest power settings (19 W), large magnitude and low frequency periodic temperature oscillations are observed.

Table 1
Relevant measurement uncertainties.

Wall Temperature	± 0.5 °C
Vapor Temperature	± 1.0 °C
Pressure	± 3%
Voltage & Current	< 0.2%

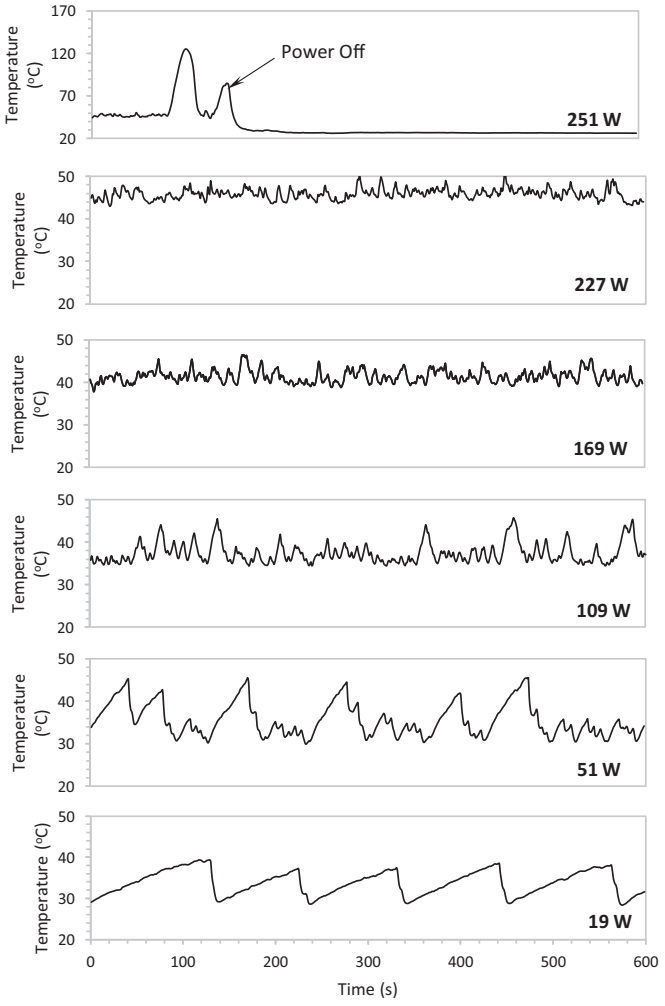

Fig. 2. Evaporator wall temperature (T_{e1}) variations with time for varying applied power.

As the power is increased to 51 W, the large oscillations are still evident though the frequency increases and they are generally separated by lower magnitude and higher frequency pulsed oscillations.

Increasing the applied power to 109 W, the magnitude of the temperature extrusions decreases and becomes less periodic and the lower amplitude oscillations become a more prominent feature of the temperature-time trace.

At 227 W and beyond the spikes in the evaporator wall temperature no longer appear and the primary feature of the temperature-time trace is that of high frequency and low amplitude oscillations that are not periodic in nature.

When the applied power is increased to 251 W the thermosyphon reaches the dryout limit as is indicated by the large temperature extrusions (noting the change in the vertical axis scale in the graph), after which the applied power is turned off.

The temperature traces in Fig. 2 are indicative of the two-phase flow patterns and the heat transfer, which of course are interdependent. One key observation here is that, regardless of applied power, the system is never steady. As the power is increased the system transitions from high amplitude, low frequency and periodic evaporator wall temperature oscillations to low amplitude, high frequency and generally non-periodic oscillations. To gain deeper insight into this behavior, the high-speed videos were examined. Figs. 3–6 are provided here to illustrate the main dynamic boiling events which were observed.

Fig. 3 shows a video sequence of a typical Geyser boiling event. This is representative of the event which is responsible for the

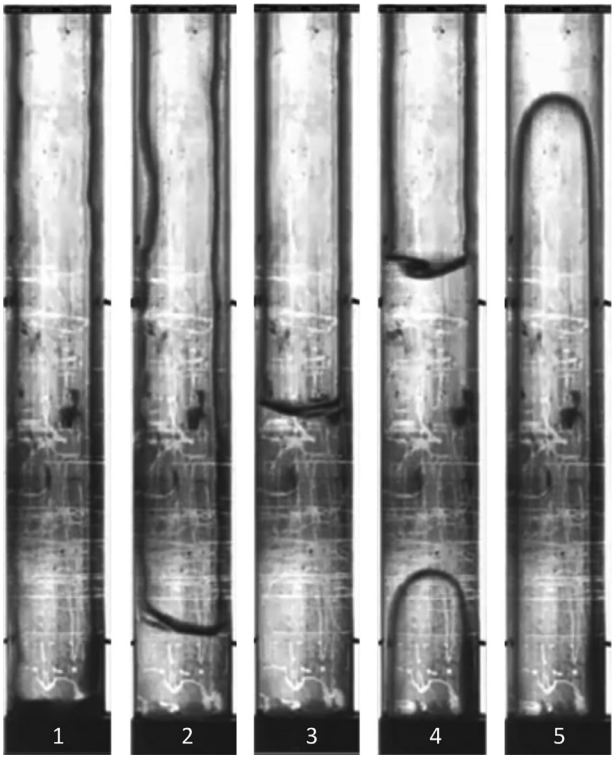

Fig. 3. Video sequence illustrating typical Geyser boiling in the evaporator; Q = 19 W.

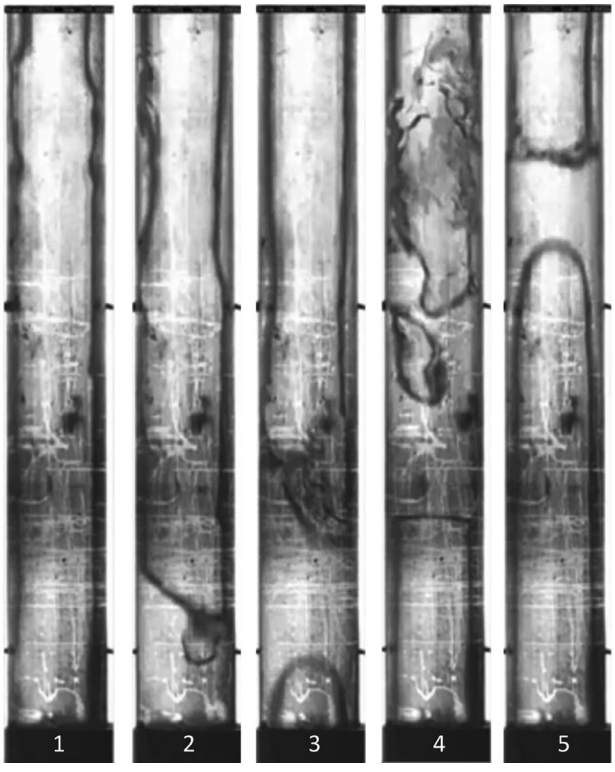

Fig. 4. Video sequence illustrating Partial Geyser boiling in the evaporator; Q = 109 W.

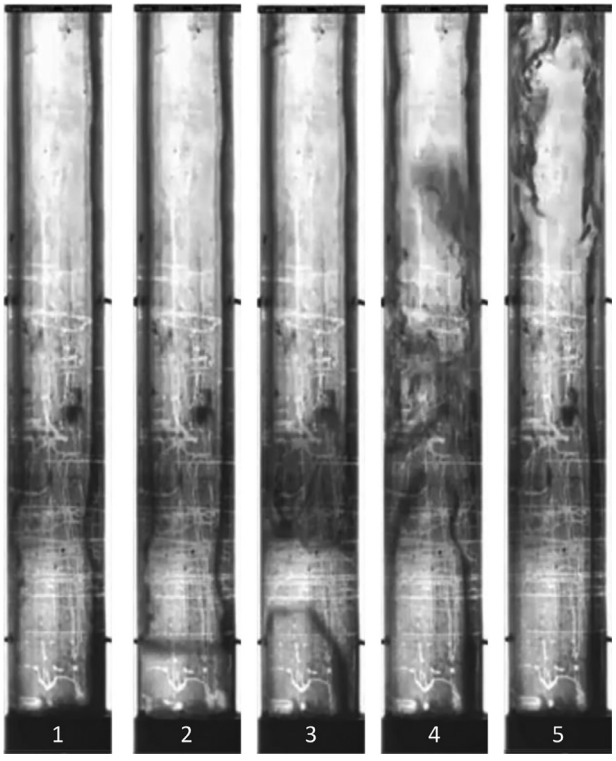

Fig. 5. Video sequence illustrating Breach boiling in the evaporator; Q = 109 W.

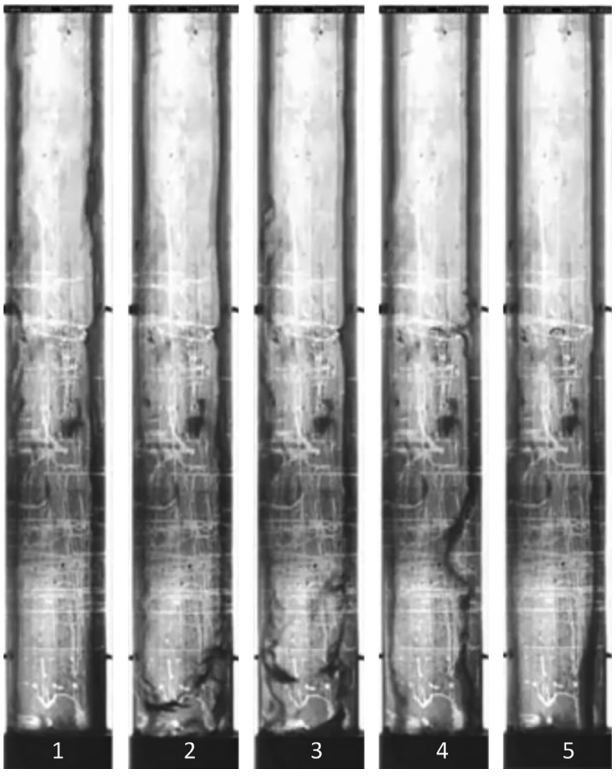

Fig. 6. Video sequence illustrating Intermittent Churn boiling in the evaporator; Q = 227 W.

large magnitude and low frequency temperature oscillations measured for the lower power settings (19 W and 51 W), shown in Fig. 2. The event begins after a prior one, whereby an elongated bubble has pushed a liquid plug into the condenser section. The sequence of Fig. 3 (1) and (2) shows the draining of the liquid, in the form of an annular liquid film, from the condenser to the evaporator. For lower power settings the draining into the evaporator continues until the filling is close to the initial fill ratio (FR = 25%), where it is noted that only about 80 mm of the 200 mm evaporator is shown in Figs. 3–6 i.e. the initial fill volume is approximately at the level of the top thermocouple shown in the photographic images.

With regard to the associated temperature histories in Fig. 2, the geysering period is associated with the relatively slow increase in the evaporator temperature. The temperature rise stops abruptly when a bubble nucleates in the lower region of the evaporator, as shown in Fig. 3 (4).

The bubble grows rapidly, and the wall temperature quickly drops accordingly, due to the high rate of evaporation across the thin annular liquid film around the bubble periphery. As Fig. 3 (4) and (5) indicate, the growing bubble forces a liquid plug upward and into the condenser (not shown). This liquid, along with any condensed vapor, then drains back to the evaporator thus beginning a new cycle. Fig. 2 shows that for 19 W of applied power the Geyser boiling regime described above is dominant, and this is confirmed in the high-speed videos shown in Fig. 3.

Increasing the power to 51 W, the temperature trace in Fig. 2 shows that the full Geyser events are separated by intermittent higher frequency and lower amplitude events. In fact, by 109 W of applied power, these latter types of events are now dominant, and the high magnitude and low frequency events have ceased.

Observation of the high-speed videos reveals that these lower amplitude temperature fluctuation events are characteristic of partial filling of the evaporator and can be separated into two distinct types; Partial Geyser and Breaching. Fig. 4 depicts an example of a Partial Geyser event for an applied power of 109 W. Here the main difference is that bubble nucleation and subsequent growth occurs when the evaporator is only filled to a small extent (FR = 5 – 10%). Still, the expanding bubble forces a small plug of liquid upward to the condenser.

The Breaching boiling event, depicted in Fig. 5, is similar to the Partial Geyser event except that the evaporator filling is less (~ 10 mm) and during bubble growth the liquid slug is ruptured, creating a churn and/or annular type of upward liquid flow. The Partial Geyser and Breaching flow regimes are typical of the events which occur between the Geyser events for 51 W of applied power. They are also typical of the moderate amplitude temperature increases observed for the 109 W and 169 W power settings (see Fig. 2).

The final boiling event type, heretofore termed Intermittent Churn, is depicted in the image sequence of Fig. 6. This type of event is associated with a low refill volume (< 10 mm) and a scenario wherein a liquid plug does not fully form during the boiling event. Here the boiling event creates a churned upward spray of liquid that splashes and wets the lower quarter section of the evaporator, with a large portion of the liquid draining back to the lower evaporator section. Here the boiling event does not propel a mass of liquid to the condenser. This event is associated with high frequency and low amplitude evaporator temperature fluctuations. Referring back to Fig. 2, this is the dominant regime for the high pre-dryout heat flux shown (227 W) and is observed down to 109 W of applied power, though not as prevalent. In the upper part of the evaporator, sporadic dry-patches are observed for the higher power settings.

Table 2 is an attempt to summarize the observed characteristic boiling events that are associated with the different applied thermal power loadings. As the table shows, the influence applied power has is progressively changing the boiling events from the large amplitude, low frequency, and periodic wall temperature fluctuations associated with Geyser boiling at low applied power, through to the low amplitude, high frequency and non-periodic fluctuations associated with Intermittent Churn boiling at high applied power. As the power is increased from the lowest to the highest setting, the boiling transition phases are associated with the intermediate Partial Geyser and Breach boiling events. It is noted here that the Intermittent Churn phase is the precursor to dryout and thus the maximum heat transfer, which was here determined to be 251 W.

3.2. Heat transfer analysis

In this section the heat transfer behavior of the thermosyphon is analyzed based on spatial and time averaged temperature measurements.

Table 2
Dominant boiling events: Green (✓) = present and/or frequent, Red (x) = not present and/or not frequent.

Power	Geyser	Partial Geyser	Breach	Intermittent Churn
19 W	✓	x	x	x
51W	✓	✓	x	x
109 W	x	✓	✓	✓
169 W	x	x	✓	✓
227 W	x	x	x	✓

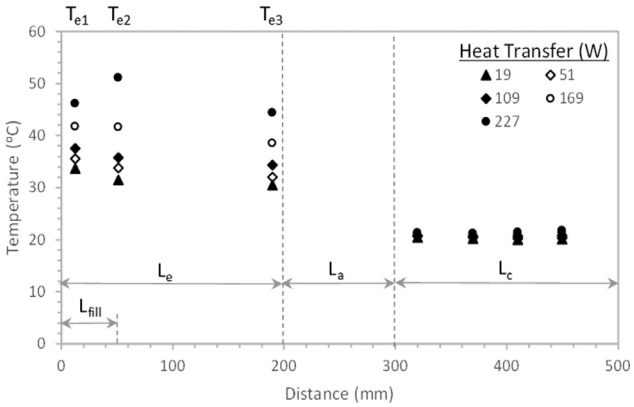

Fig. 7. Wall temperature distribution for varying applied power.

Fig. 7 shows the temperature distribution along the thermosyphon for varying applied power. As it is shown, the condenser wall temperature is uniform and independent of applied power, remaining about 20 °C for each test. As discussed earlier, this is due to the high setting of water flow rate on in the water jacket such that the condenser wall temperature assumes that of the coolant.

For power levels between 19 W and 169 W the evaporator temperature is relatively uniform, though with a slight downward trend. Increasing the applied power causes the evaporator wall temperature to increase monotonically. For the high pre-dryout heat transfer of 227 W, T_{e2} is notably above that of T_{e1} and T_{e3}, and is indicative of some local dryout events, and this is consistent with the observations of Jafari et al. [15].

At the top of the evaporator, condensate which is drained from the condenser, serves to keep this top region wetted. However, the liquid film thickness decreases moving downward toward the evaporator causing intermittent local dry patches and thus decreased heat transfer effectiveness.

In the bottom section, as noted earlier, a small pool of liquid collects and the Intermittent Churn boiling events serve to splash and wet the lower region resulting in better heat transfer effectiveness and thus lower wall temperatures. Fig. 8 plots the spatial and time averaged heat transfer coefficient for increasing applied thermal power for both the evaporator and condenser sections. Fig. 8(a) shows that the heat transfer coefficient in the evaporator escalates nearly linearly with applied power up to 211 W. Beyond this h_e decreases, and this is largely due to the increase in T_{e2} for reasons discussed above.

This decline in h_e is an indicator of the thermosyphon approaching full dryout and ultimate failure, which here occurs at 251 W.

A short discussion is warranted regarding the magnitude of the evaporator heat transfer coefficients. Fig. 8(a) shows that it ranges between ~ 2,000 W/m^{2}K at 19 W (3.75 kW/m^2) and 20,000 W/m^{2}K at 202 W (40.3 kW/m^2). For a point of reference, the Imura correlation [16] can be considered as it has been shown time and again to accurately predict nucleate pool boiling heat transfer coefficients in reflux thermosyphons and is typically used as the *de facto* comparison

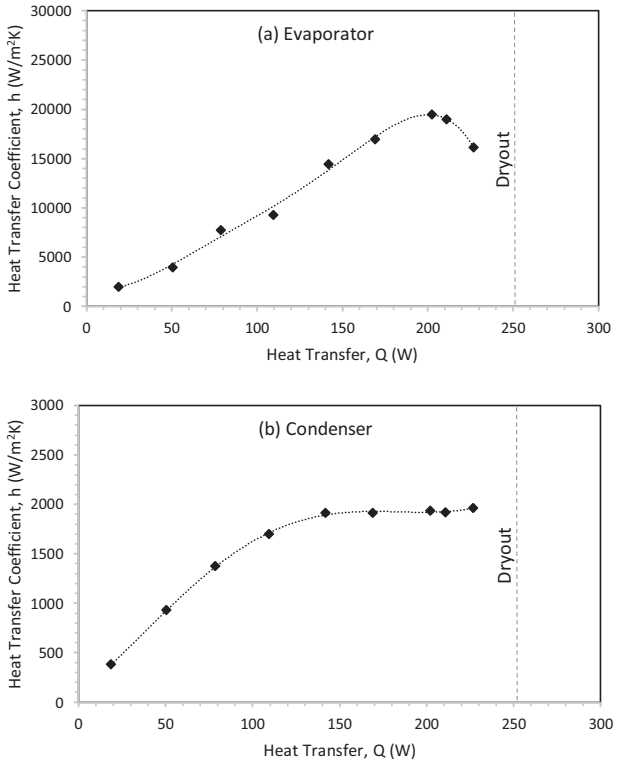

Fig. 8. Heat transfer coefficient as a function of applied thermal power (a) evaporator, (b) condenser.

correlation for determining the relative evaporator performance of thermosyphons.

Utilizing the Imura correlation predicts evaporator heat transfer coefficients in the range of 1800 – 5500 W/m^2 for the range of heat fluxes tested. This is notably lower than the measured heat transfer coefficients shown in Fig. 8(a), which range between 2,000–20,000 W/m^2.

The main reason for this is the difference in the boiling dynamics in the evaporator. For this thermosyphon, there is no visual evidence of a nucleate pool boiling regime. On the contrary, the primary heat transfer mechanisms are associated with thin film evaporation, during the drainage phase Figs. 3–6 ((1)) followed by rapid boiling events that themselves tend to result in thin film evaporation Figs. 3–6 ((5)). Thus, one would expect a notably higher evaporator heat transfer coefficient than that associated with pool boiling. In fact, as the applied power is increased and the average time during which thin film evaporation occurs also increases, the magnitude of the heat transfer coefficient would be expected to approach that which is commensurate with annular flow boiling opposed to nucleate boiling. For annular flow boiling, heat transfer coefficients are of the order of 10,000 – 20,000 W/m^{2}K for water [19], which is consistent with the order of magnitude measured in this work for mid to high heat fluxes i.e. when Geysering is not a dominant flow feature. Therefore, it can be speculated that the low fill volume of this thermosyphon is conducive to high evaporator heat transfer coefficients because it incurs thin film evaporation as a dominant mechanism of heat transfer. The drawback, however, is that the thin film tends to dryout at fairly moderate heat fluxes, here a maximum of 50 kW/m^2, which thus limits its operation.

In Smith et al. [11], where the 100 mm evaporator length was used with FR = 100%, the evaporator heat transfer coefficients were generally lower than the Imura predictions, being 500 – 5000 kW/m^2 for a heat flux range of 7.5 – 63 kW/m^2, due to the predominance of Geyser boiling. Again, the h_e measurement for the current low FR = 25% and L_e = 200 mm are significantly higher than the same experiment as Smith et al. [11] though now with the longer evaporator length and lower filling ratio. Again, this can be accounted for by a difference in the boiling regimes, though now associated with the fill ratio effect. In the present work, the low fill ratio results in a significant portion of the evaporator experiencing the very effective thin film evaporation mode of heat transfer, even within the Geyser regime, whereas the earlier work with 100% fill ratio did not. To the best of knowledge, this is a novel finding, in that the influence of fill ratio on the heat transfer effectiveness of Geyser boiling in the evaporator has not been significantly explored in confined thermosyphons. In a recent in depth review of boiling heat transfer in reflux thermosyphons, Guichet et al. [20] discuss correlations for different boiling modes, including nucleate boiling, thin film boiling and geyser boiling. Of the correlations that exist for geyser boiling, that of Casarosa and Latrofa [21] is suggested;

$$h_e = 2.925 P_v^{0.18} q_e^{2/3} \tag{11}$$

However, this correlation predicts evaporator heat transfer coefficients in the range of 400–2500 W/m^{2}K, which significantly under predicts the current values, though is remarkably close to the range of the earlier Smith et al. [11] work. Both of these works used FR=100%, thus illustrating that Geyser boiling heat transfer effectiveness can be improved significantly using low fill ratios.

With regard to effect of confinement, there is little work available with respect to predicting heat transfer coefficients in reflux thermosyphons. Guichet et al. [20] discuss confinement in the context of nucleate boiling and its influence on bubbles, particularly bubble coalescence, which is not relevant here. However, a recent publication by Padovan et al. [22] specifically addresses confinement effects on reflux thermosyphons. Here, a thermosyphon typically used in solar thermal collectors, with an inside diameter of 6.4 mm, was tested with water as the working fluid. As such the Confinement Number is commensurate with the study here. Although the evaporator was quite long (~1 m), the fill ratio was low (FR=16%). The investigation showed that conventional heat transfer correlations could not predict their experimental measurements for the heat transfer in the evaporator and they proposed a new correlation for the evaporator heat transfer coefficient in confined thermosyphons as;

$$h_e = 2321 P_r^{0.23} M^{-0.93} Bo^{0.14} q_e^{0.41} \tag{12}$$

Here the Bond number, Bo, accounts for confinement since it can easily be shown that Co=Bo$^{-1/2}$. Applying this correlation with the present data once again significantly under predicts the measurements here, with predicted heat transfer coefficients ranging between 850 and 3000 W/m^{2}K. Although the Padovan et al. [22] work specifically addresses confinement in reflux thermosyphons, it is more consistent with the prediction of the Casarosa et al. [21] geyser boiling correlation, which may be due to the low heat fluxes tested ($\leq$8 kW/m^2) or due to the large evaporator length to diameter ratio, which was 166 compared to 25 in the present study. Regardless, the results of the present work, based on visual observation and order of magnitude of the calculated heat transfer coefficients, support the hypothesis that the primary mechanism of heat transfer for the low filling ratio and confined thermosyphons tested here is akin to annular flow in convective flow boiling, and an adequate correlation to predict the heat transfer does not appear to exist in the literature. This highlights that there are still significant gaps in knowledge with regard to thermosyphon science and technology and there is still much work to be done with regard to developing robust flow regime maps and accurate heat transfer correlations for the associated flow regimes. Although the recent works of Smith et al. [10,11] is a start to this progress, it considered a limited range of parameters and a full understanding must expand significantly upon this including but not limited to confinement, fill ratio, length to diameter ratio, heat flux and operating pressure.

Fig. 8(b) shows the trend associated with the condenser heat transfer coefficient with increasing applied thermal power. In contrast to

the evaporator, the trend in the condenser is asymptotic, which begins at ~ 400 W/m^{2}K for the lowest heat flux and plateaus at ~ 2000 W/m^{2}K. The heat transfer coefficient is low at these heat transfer rates as much of the heat transfer between the evaporator and condenser is by sensible heat stored in the liquid plug that is pushed into the condenser during the Geysering events. For the mid to high heat fluxes the liquid transport to the condenser is in the form of a churned mass. This, and the higher amount of latent heat transport to the condenser via the up-flowing vapor, results in improved heat transfer compared with that associated with Geysering.

With regard to the overall magnitude of the condenser heat transfer coefficient, it is prudent to compare it with that of Nusselt's falling film theory, which predicts condensation heat transfer coefficients in the range of 6000−7000 W/m^{2}K for the range of heat fluxes tested. The measurements here are well below the Nusselt falling film prediction; by an order of magnitude at the lowest heat flux and by a factor of 3 at mid to high heat fluxes. Though previous studies have shown that for small diameter thermosyphons the Nusselt falling film theory can significantly over predict the measured heat transfer coefficient [23,24], the exact mechanism was not clear. In this work, as the heat flux is increased, progressively more heat is transferred from the evaporator to the condenser by latent heat, opposed to sensible heat in the liquid slugs, which improves the effectiveness of heat transfer, though not to the extent of reaching that of falling film condensation. The reason for this is liquid hold-up in the condenser, as discussed by Smith et al. [10]. For thermal power loads above about 100 W (~22 kW/m^2), it is observed that only a small volume of liquid is drained back to the evaporator meaning that a high liquid volume is held in the condenser by the high upward vapor momentum. As such the effective area of the condenser is reduced which limits its overall effectiveness.

In the context of thermosyphon thermal performance, it is significant that the condenser heat transfer coefficient is much lower than that of the evaporator, in the sense that it becomes the dominant thermal resistance of the thermosyphon for the case here where their surface areas are equivalent. This is highlighted in Fig. 9 where the total effective thermal resistance is plotted along with the constituent evaporator and condenser resistances. As it is shown, the dominant thermal resistance is associated with the condenser.

Considering the above discussion, an interesting result here is that the low fill volume of this small diameter thermosyphon has the benefit of creating a low thermal resistance in the evaporator, which is limiting due to dryout of the thin liquid film which tends to dominate the heat transfer at the higher heat fluxes. Thus, the evaporator ultimately limits the maximum heat transport capacity. On the other hand, the condenser plays a role in limiting overall thermal resistance due to sensible heat transfer at lower heat fluxes and liquid hold-up at higher heat fluxes.

Overall, an important observation here is that the mechanisms of heat transfer in the condenser are not nearly as effective as that of the evaporator and much below that of the ideal case of falling film condensation. In this context, in engineering an enhanced small diameter thermosyphons, it is prudent to focus on the condenser and methods which improve the effectiveness of heat transfer whilst promoting liquid drainage to the evaporator. If a technology or technique could be engineered to mitigate liquid hold-up, it would have the benefit of reducing the thermal resistance of the condenser whilst at the same time promoting drainage of liquid to the evaporator which should mitigate dryout and increase the maximum power limit. For example, there has been some previous work on surface modifications on the condenser walls to change the wetting characteristics [25-28]. However, these works have focused on larger diameter (unconfined) thermosyphons with the aim to use hydrophopic coatings to promote dropwise condensation and improve the heat transfer effectiveness. It is possible that similar techniques could be used for confined thermosyphons to mitigate liquid hold-up.

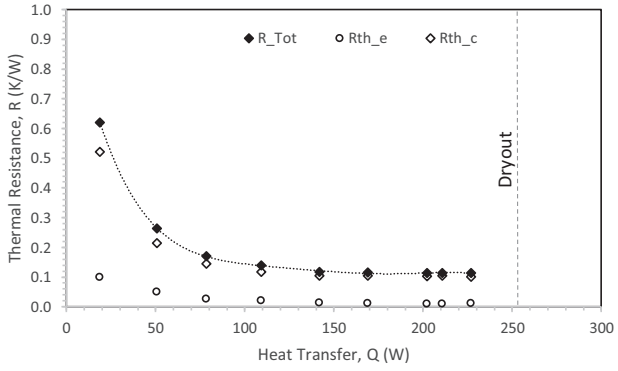

Fig. 9. Thermal resistance variation with applied heat loads.

4. Conclusion

This work presents an experimental investigation of a reflux two-phase thermosyphon. The thermosyphon is charged with water as the working fluid with what can be considered a low fill volume ratio of FR = 25% for a relatively long evaporator length of 200 mm. With water as the working fluid, the small diameter (8 mm) thermosyphon can be considered confined since the Confinement Number is Co ~ 0.34, meaning that the capillary length of the water is about one-third of the thermosyphon inner diameter. Importantly, the transparent sapphire thermosyphon container material allows visual access to the two-phase flow dynamics in the evaporator section.

By progressively increasing the applied heat flux it was determined that the heat and mass transfer behavior of the thermosyphon is never quasi-steady. For low heat fluxes, Geyser boiling is prominent whereby nearly the entire volume of fluid is drained to the evaporator between Geyser events. This results in evaporator wall temperature fluctuations which are large in magnitude, low in frequency and periodic in nature. Ultimately, the heat transfer coefficients in the evaporator and condenser are at their lowest. As the heat flux is increased, progressively less liquid is drained back to the evaporator subsequent to boiling events which results in flow regimes that are associated with lower amplitude evaporator temperature fluctuation of higher frequency which lack periodicity. Here the effectiveness of the heat transfer in the evaporator improves considerably as the dominant mechanism of heat transfer becomes that of evaporation of a thin liquid film. The condenser heat transfer also improves as a higher proportion of heat transfer between the evaporator and condenser is by latent heat opposed to sensible heat, with the latter being the result of for Geyser boiling. Even still, the condenser heat transfer effectiveness appears to be limited by liquid hold-up which reduces its effective condenser length and thus heat transfer area.

One main finding is that the condenser dynamics play an important role both with regard to the overall thermal resistance and the maximum heat load capacity. For the former, the mode of heat transfer is not falling film condensation which has the effect of causing it to be the dominant thermal resistance. Furthermore, liquid hold-up resulting from the relatively low volume of working fluid combined with the high vapor momentum at mid to high heat loads, has the end effect of starving the evaporator of liquid thus promoting dryout and ultimate failure. Future engineering research should thus focus on solutions which promote drainage of liquid from the condenser to the evaporator which may lower the condenser thermal resistance and increase the maximum heat transfer capacity.

Declaration of Competing Interest

The authors have no competing interests to declare.

References

[1] D. Jafari, A. Franco, S. Filippeschi, P. Di Marco, Two-phase closed thermosyphons: a review of studies and solar applications, Renew. Sustain. Energy Rev. 53 (2016) 575–593.

[2] K. Smith, S. Siedel, A.J. Robinson, R. Kempers, The effects of bend angle and fill ratio on the performance of a naturally aspirated thermosyphon, Appl. Therm. Eng. 101 (2016) 455–467.

[3] L.L. Vasiliev, S. Kakaç, Heat Pipes and Solid Sorption Transformations: Fundamentals and Practical Applications, CRC Press, 2013.

[4] J. Xiang, C. Zhang, C. Zhou, J. Huang, G. Liu, H. Zhao, An integrated radial heat sink with thermosyphon for high-power LEDs applications, Heat Mass Transf. 55 (2019) 2455–2467.

[5] H. Mroue, J.B. Ramos, L.C. Wrobel, H. Jouhara, Performance evaluation of a multi-pass air-to-water thermosyphon-based heat exchanger, Energy 139 (2017) 1243–1260.

[6] W. Kong, Z. Wang, X. Li, G. Yuan, J. Fan, B. Perers, S. Furbo, Test method for evaluating and predicting thermal performance of thermosyphon solar domestic hot water system, Appl. Therm. Eng. 146 (2019) 12–20.

[7] M. Narcy, S. Lips, V. Sartre, Experimental investigation of a confined flat two-phase thermosyphon for electronics cooling, Exp. Therm. Fluid Sci. 96 (2018) 516–529.

[8] K. Cornwell, P.A. Kew, Boiling in small parallel channels, in: P.A. Pilavachi (Ed.), Energy Efficiency in Process Technology, Springer Netherlands, Dordrecht, 1993, pp. 624–638.

[9] C.L. Ong, J.R. Thome, Macro-to-microchannel transition in two-phase flow: part 1 – Two-phase flow patterns and film thickness measurements, Exp. Therm. Fluid Sci. 35 (1) (2011) 37–47.

[10] K. Smith, R. Kempers, A.J. Robinson, Confinement and vapour production rate influences in closed two-phase reflux thermosyphons part A: flow regimes, Int. J. Heat Mass Transf. 119 (2018) 907–921.

[11] K. Smith, A.J. Robinson, R. Kempers, Confinement and vapour production rate influences in closed two-phase reflux thermosyphons part B: heat transfer, Int. J. Heat Mass Transf. 120 (2018) 1241–1254.

[12] Y. Kim, D.H. Shin, J.S. Kim, S.M. You, J. Lee, Boiling and condensation heat transfer of inclined two-phase closed thermosyphon with various filling ratios, Appl. Therm. Eng. 145 (2018) 328–342.

[13] B. Jiao, L.M. Qiu, X.B. Zhang, Y. Zhang, Investigation on the effect of filling ratio on the steady-state heat transfer performance of a vertical two-phase closed thermosyphon, Appl. Therm. Eng. 28 (2008) 1417–1426.

[14] H. Shabgard, B. Xiao, A. Faghri, R. Gupta, W. Weissman, Thermal characteristics of a closed thermosyphon under various filling conditions, Int. J. Heat Mass Transf. 70 (2014) 91–102.

[15] D. Jafari, S. Filippeschi, A. Franco, P. Di Marco, Unsteady experimental and numerical analysis of a two-phase closed thermosyphon at different filling ratios, Exp. Therm. Fluid Sci. 81 (2017) 164–174.

[16] H. Imura, H. Kusuda, J.I. Ogata, T. Miyazaki, N. Sakamoto, Heat transfer in two-phase closed-type thermosyphons, JSME Trans. 45 (1979) 712–722.

[17] D.A. Reay, P.A. Kew, Heat pipes: theory, design and applications, Fifth edition, Butterworth-Heinemann, 2006.

[18] S.J. Kline, F.A. McClintock, Describing uncertainties in single-sample experiments, Mech. Eng. 75 (1) (1953) 3–8.

[19] S.-.M. Kim, I. Mudawar, Theoretical model for local heat transfer coefficient for annular flow boiling in circular mini/micro-channels, Int. J. Heat Mass Transf. 73 (2014) 731–742.

[20] V. Guichet, S. Almahmoud, H. Jouhara, Nucleate pool boiling heat transfer in wickless heat pipes (two-phase closed thermosyphons): a critical review of correlations, Therm. Sci. Eng. Prog. 13 (2019) 100384.

[21] C. Casarosa, E. Latrofa, A. Shelginski, The geyser effect in a two-phase thermosyphon, Int. J. Heat Mass Transf. 26 (6) (1983) 933–941.

[22] A. Padovan, S. Bortolin, M. Rossato, S. Filippeschi, D. Del Col, Vaporization heat transfer in a small diameter closed two-phase thermosyphon, J. Heat Transf. 141 (9) (2019) 091811.

[23] H. Hashimoto, F. Kaminaga, Heat transfer characteristics in a condenser of closed two-phase thermosyphon: effect of entrainment on heat transfer deterioration, Heat Transf. Res. 31 (2) (2002) 212–225.

[24] H. Jouhara, A.J. Robinson, Experimental investigation of small diameter two-phase closed thermosyphons charged with water, FC-84, FC-77 and FC-3283, Appl. Therm. Eng. 30 (2–3) (2010) 201–211.

[25] P. Zhang, F.Y. Lv, A. Askounis, D. Orejon, B. Shen, Role of impregnated lubricant in enhancing thermosyphon performance, Int. J. Heat Mass Transf. 109 (2017) 1229–1238.

[26] M. Rahimi, K. Asgary, S. Jesri, Thermal characteristics of a resurfaced condenser and evaporator closed two-phase thermosyphon, Int. Commun. Heat Mass Transf. 37 (2010) 703–710.

[27] Z. Zhao, P. Jiang, Y. Zhou, Y. Zhang, Y. Zhang, Heat transfer characteristics of two-phase closed thermosyphons modified with inner surfaces of various wettabilities, Int. Commun. Heat Mass Transf. 103 (2019) 100–109.

[28] Y. Kim, J.S. Kim, D.H. Shin, J.H. Seo, S.M. You, J. Lee, Effects of hydrophobic and superhydrophobic coatings of a condenser on the thermal performance of a two-phase closed thermosyphon, Int. J. Heat Mass Transf. 144 (2019) 118706.